CCFE
CULHAM CENTRE FOR FUSION ENERGY

UK Atomic Energy Authority

UKAEA-CCFE-PR(19)14

Luc Andre, Kathrin Abraham, Axel Hofmann,
Laurence Monin, Ilka C. Kleinhanns, Stephen Foley

Origin of Early Continental Crust by Reworking Silicified Metabasalts

Origin of Early Continental Crust by Reworking Silicified Metabasalts

Luc Andre, Kathrin Abraham, Axel Hofmann, Laurence Monin,
Ilka C. Kleinhanns, Stephen Foley

This is a preprint of a paper submitted for publication in
Nature Scientific Reports

ORIGIN OF EARLY CONTINENTAL CRUST BY REWORKING SILICIFIED METABASALTS

Luc André*, Kathrin Abraham, Axel Hofmann, Laurence Monin, Ilka C. Kleinhanns, Stephen Foley

ABSTRACT

How the Archean felsic crust grew from its mafic precursors between 3.8 and 2.5 billion years ago remains elusive and the subject of great debate. Here, we present silicon isotopic constraints on Tonalite-Trondhjemite-Granodiorite (TTG) and Granite-Monzonite-Syenite (GMS) plutons from the Kaapvaal craton, which range in age from 3.55 to 2.69 Ga. We identified very consistent isotopic signatures (TTG: δ^{30}Si=+0.01±0.11‰; GMS: δ^{30}Si=-0.03±0.11‰), all uniformly heavier than those ever determined for rocks which comprise most of the Bulk Silicate Earth, the Si-rich end-members of the modern continental crust and dacite-rhyolite liquids differentiated from basalts. This unusual composition is explained by the melting of a mafic source that included significant proportions (20-35wt%) of silicified metabasalts, which were common supracrustal rocks prior to 3 billion years. Thus, differentiation of the early continental crust may have been enabled by enrichment of the mafic source rocks in silica from interaction with silica-saturated early oceans prior to the melting event that formed the granitoids. Addition of silica depresses the stability of amphibole at similar water activity, allowing TTG-like melt production at lower temperatures. This may explain why early silicic continental granitoids are unique to Earth and did not emerge on other rocky planets.

*Corresponding author

The Earth is unique among the rocky planets of the solar system in possessing a thick felsic continental crust. A number of recent models[1-4] are converging to indicate that the continental crust formed very early in the Earth history and had 30-70% of its present volume by 3 Ga depending of the rate of crustal recycling[4]. Granitoids of the TTG and GMS suites compose the bulk of this early phase of continental growth. Establishing how these granitoid rocks were formed, and determining how their petrological differences occurred, are critical for understanding how continental crust grew in this early phase and why it is unique among the rocky planets. Silicon is the most abundant cation in the Earth's continental crust[5]. As such, it is the major characteristic feature that distinguishes the continental crust from the other major Earth reservoirs. Defining the source of silicon in the early crustal TTGs and GMSs through a study of their isotopic composition (δ^{30}Si) is therefore a potential way for tracking how the continents initially formed.

The main silicate reservoirs in the Earth have quite similar average Si isotopic compositions. In particular, basaltic melts (δ^{30}Si= –0.32±0.12‰ average of ref 6-7) do not actually differ from their mantle-source reservoirs (−0.29±0.08‰)[6,8], but their differentiated melts become very slightly enriched in heavy silicon (up to a maximum δ^{30}Si≈-0.14‰) due to the small bulk $\Delta Si_{solid\text{-}melt}$ isotopic fractionations (≈-0.125‰)[9]. Together these rocks define an "igneous array" (Fig. 1A), which describes the predicted changes of Si isotopic composition as a function of the silica content of melts[6,9]. With the prominent exception of sediment-derived peraluminous leucogranites[10-11] and a few andesites[11], all Phanerozoic Si-rich rocks (SiO_2>55wt%) fit this igneous array trend (Fig. 1A). In contrast to these rather isotopically uniform igneous reservoirs, the supracrustal domains exhibit significant Si isotopic differentiations of up to 10 ‰ due to large equilibrium and kinetic isotopic fractionation between phases at low temperatures[12,13]. This is the consequence of preferential

*Corresponding author

46 incorporation of light isotopes (^{28,29}Si) in precipitated secondary minerals[13], biogenic silica[12],
47 clays and their derivative fine-grained sediments[14], all three of which are counterbalanced
48 by the relative enrichment of ^{30}Si in the water-dissolved silicon fractions. These diverse
49 mineral-fluid interactions converge to make the global hydrosphere the principle terrestrial
50 ^{30}Si-rich reservoir. Hence, silicon isotopes have the great advantage of uniquely
51 differentiating between water-derived precipitates from clay-derived sediments.

52 Precambrian Si-rich seawater deposits include Banded Iron Formation (BIF) and cherts.
53 These differ strongly in their Si isotopic compositions[15,16]: Si In BIF is usually light (mean δ^{30}Si
54 at -1.1‰[16]), while cherts are mostly heavy (mean δ^{30}Si at +0.8‰[16] Fig. 1B). However, as
55 recently recognised by Zheng et al.[16], both likely precipitated from a common oceanic
56 reservoir with heavy Si isotopes through contrasting isotopic fractionations, because the
57 combined Fe-Si gel precursors of BIF[16,17] display $\Delta^{30}Si_{gel\text{-}aqueous}$ twice the magnitude of pure Si
58 gels from which cherts were likely deposited[16]. During the Eo- to Paleoarchean, the paucity
59 of emerged continents limited a soil-derived silicon flux to seawater. Oceanic silicon input
60 was mostly from the leaching of Si from oceanic crust by hydrothermal alteration instead.
61 Input is considered to have been equal to Si removals through the silicification of oceanic
62 substrate and the deposition of amorphous silica associated with BIF and chert on the
63 seafloor[18,19]. By mass balance this implies that both the precipitated silica and the remaining
64 Si-saturated seawater would have developed higher δ^{30}Si through time[18,19]. In parallel,
65 because they reacted with heavy seawater Si, the silicification of Archean basaltic seafloors
66 caused them to acquire bulk positive heavy Si isotopic compositions[20]. Therefore, Si isotopes
67 have a great potential to fingerprint the source of Archean granitoids by distinguishing
68 between potential contributions from BIF, shale, igneous rock, silicified metabasalt, and
69 chert, in a grading scale from negative to positive δ^{30}Si signatures. A crucial factor is the ~~the~~

*Corresponding author

strong resistance of these differentiated supracrustal silicon isotopic signatures to metamorphic equilibration up to high temperature (>700°C)[21]. This explains why these signatures can survive unchanged to depths where melting can occur[10-11].

Representative granitoid rocks from the Barberton Greenstone Belt (BGB) of the Kaapvaal craton were selected to encompass the Archean progression from early TTG plutons (3.51-3.11Ga; mostly trondhjemitic Na-rich granitoids) to later GMS plutons (3.20-2.69Ga, mostly K-rich granites). Their Ab-An-Or compositions are illustrated in the supplementary Fig.1 and the geographic coordinates of the sample locations are listed in supplementary Table 1. $\delta^{30}Si$ and $\delta^{29}Si$ for all samples as well as the pluton ages and some key geochemical features (SiO_2, K_2O/Na_2O, Eu/Eu*, La_N/Yb_N, Sr/Y, Lu/Hf) are summarized in Supplementary Table 2. In terms of their average $\delta^{30}Si$, there are no resolvable differences between TTG and GMS samples at +0.01±0.11‰ (±2SD, n=15) and -0.03±0.11‰ (±2SD, n=22), respectively. In the $\delta^{30}Si$ vs SiO_2 diagram (Fig. 1B), they plot clearly above the "igneous array", being significantly heavier than both Phanerozoic I and A type granites ($\delta^{30}Si$=–0.19±0.08‰[10,11]) as well as dacite-rhyolite melts differentiated from basalts ($\delta^{30}Si$=–0.17±0.08‰[9,22]).

ORIGIN OF THE HEAVY SI ISOTOPIC SIGNATURE OF TTG.

Two main families of models have been proposed for the origin of TTG magmas: (1) melting of metabasalts recycled into the mantle or reworked at the base of a thickened basaltic crust[23]; (2) fractionation of hydrous basalts[24]. In both cases, garnet and/or amphibole play a key role in shaping the geochemistry of the melts, especially in producing their characteristic fractionations of light from heavy REE (La_N/Yb_N) as well as of Sr relative to Y. Both garnet and amphibole could preferentially incorporate the light Si isotope relative to

*Corresponding author

93 quartz[25] and it has been calculated[26] that a melt produced by low-degree melting of eclogite
94 might bear heavier Si isotopic values (-0.13<δ^{30}Si<-0.07‰), close to the range of what we
95 observe for the Barberton TTGs. However, because we do not see any variation of δ^{30}Si as a
96 function of the large variation in La_N/Yb_N (5 to 68) and Sr/Y (22 to 228) found in the studied
97 TTGs (Supplementary Fig. 2A,B), partial melting or fractional crystallisation involving garnet
98 or amphibole can be ruled out as the major cause for the recorded heavy Si isotopic
99 signatures.

100 Thermal diffusion is another means to cause changes in Si isotopes, with ^{30}Si being
101 consistently enriched toward the cold end of the system[27]. So, the heavy Si isotopic
102 composition of TTGs would be consistent with a thermal diffusion-controlled isotopic
103 fractionation, whereby δ^{30}Si increases with cooling at decreasing depth. However, in the
104 three natural occurrences of felsic rocks where a possible diffusion-related fractionation has
105 been proposed, the Torres del Paine Pluton[28], the Cedar Butte volcano and the Duluth
106 Complex[22], the silicon isotopic composition of the felsic components remains in the range of
107 the igneous array (Fig. 1B). Furthermore, if thermal diffusion-controlled fractionation were
108 to account for the high δ^{30}Si of the Barberton granitoids, it is unclear why these differ from
109 Phanerozoic granitoids. Our conclusion is that thermal diffusion generates quite limited Si
110 isotopic fractionation and is far from sufficient to account for the observed high δ^{30}Si values.

111 Crustal assimilation by granitoid melts of all types is widespread and has to be
112 considered as a possible cause of the observed heavy Si isotopic composition of TTGs. Cherts
113 are well represented within the 18-km thick BGB Onverwacht Group in which most of the
114 studied TTGs were intruded[29]. Their variable but generally heavy Si isotopic signatures (Fig.
115 1B) identify them as possible contaminants, especially given the presence of chert xenoliths

116 in some TTG plutons[30]. The heat required for assimilation can be provided by the latent heat
117 of crystallization of the magma, and this coupling should trigger an increase in the silica
118 proportion of the more differentiated products[31]. The assimilation of cherts should therefore
119 drastically increase the proportion of silica in the residual melt, with the consequence of a
120 positive rough trend between δ^{30}Si and SiO_2 contents in TTGs. Instead, we observe a slightly
121 negative δ^{30}Si-SiO_2 correlation ($\delta^{30}Si=-0.0094xSiO_2+0.6477$, Fig. 1B), which precludes
122 contamination of this type, because it would imply an unrealistic specific chert contaminant
123 with a locally seldom low δ^{30}Si (≈–0.25‰).

124 Basalts from the Onverwacht Group bear average mantle-like signatures (δ^{30}Si= -
125 0.30±0.14‰, $\pm 2\sigma_{\bar{X}}$)[20], although δ^{30}Si values are more scattered compared to their modern
126 equivalents due to hydrothermal and metamorphic overprints. In contrast, the silicified
127 portions of Onverwacht Group seafloor basalts have thoroughly modified ^{30}Si-enriched
128 seawater-derived isotopic signatures (δ^{30}Si=+0.43±0.14‰, $\pm 2\sigma_{\bar{X}}$)[20]. In a δ^{30}Si-SiO_2 diagram
129 (Fig. 1B) Barberton TTGs plot to the right of the array designed by unsilicified and silicified
130 pillow basalts and associated cherts. This observation supports the hypothesis of TTG
131 derivation by melting of a stack of variably silicified metabasaltic rocks that were
132 geodynamically placed into appropriate P-T conditions for melting because the melting
133 process would enrich the liquids in silica with limited Si isotopic fractionations (~0.1‰)[9]
134 pushing the data laterally to the right of the metabasalt array. It is worth mentioning that all
135 early Archaean rocks exposed to seafloor conditions (including ultramafic and felsic
136 volcanics) were prone to silicification[29], but we focus our discussion on basalts because they
137 are the most common rocks in greenstone belts[32]. Cherts must have contributed to the
138 metabasaltic mixture, but only to a small extent, because the chert horizons interlayered
139 between the basaltic lava flows are volumetrically minor in comparison to the silicified

metabasalts. Their average Si isotopic compositions (δ^{30}Si=+0.39±0.17‰, $\pm 2\sigma_{\bar{X}}$)[20] are in the exact range of the silicified metabasalts (Fig. 1B), so that their contribution is effectively included in the weighted average of silicified metabasalts.

Using the average compositions of Theespruit metabasalts (~3.54 Ga) which predate all studied TTGs (3.5-3.1 Ga) as a potential source of mixed silicified and unsilicified end-members (Supplementary Table 3), ~~modeled~~modelled mixtures including about 20-35% of silicified metabasalts (Supplementary Fig. 3) would account for both K_2O/Na_2O and δ^{30}Si TTG's properties. Using phase equilibria modeling, Johnson et al.[33] recently constrained the origin of TTGs from the Pilbara craton as produced by 20-30% melting of low-MgO tholeiites of the ~3.5Ga Coucal Formation at the base of the Pilbara Supergroup. A mixture incorporating a 1:3 ratio of silicified and unsilicified Theespruit metabasalts has a major element composition similar to the average of the Coucal basalts (C-F2)[33] (Supplementary Table 3). In particular, its intermediate SiO_2 content (54.7 wt%), low MgO content (5.6wt%) and low K_2O/Na_2O ratio (0.11) supports this assemblage as a suitable source-rock from which TTG-like melts could be extracted at realistic geothermal gradients (700-1100°C GPa^{-1})[33].

All Theespruit silicified and unsilicified metabasalts present low Lu/Hf (Fig. 2) which mimic the one found for the Coucal basalt (0.12, Supplementary Table 3). This is another key point because a source with such low Lu/Hf relative to N-MORB (0.195) is necessary to account for the very low Lu/Hf characteristics (0.035 on average) of early Earth TTGs[34,35]. This is likely the consequence of the preferential depletion of Lu relative to Hf during basalt alteration[29], which is especially amplified in silicified portions of the Onverwacht Group with the highest δ^{30}Si (Fig. 2). Therefore we are confident that the 1:3 ratio of silicified and unsilicified Theespruit metabasalts constitutes a robust source-type for the Barberton TTGs.

*Corresponding author

SILICIFYING A METABASALT SOURCE PROMOTES TTG MELTS.

Rock compositions with higher SiO_2 have more restricted amphibole stability at similar water activity[36]. Since TTG-like crust is formed by melting of garnet amphibolite[37], the addition of SiO_2 permits melting at lower temperatures (≈100˚C)[38], at the low MgO content[33] consecutive to the silicification. This allows TTG production earlier in time when much of the MgO-rich crust may have been incapable of producing TTG melts[37]. By facilitating the garnet crystallisation it also causes plagioclase to be a reactant leaving more Na available for the produced TTG-like melts[38]. This would apply to the silicified basaltic source considered here with 54-55wt% SiO_2, whereas melting of amphibolites with still higher SiO_2 (60wt%) generates granodioritic-granitic melts with K/Na higher than trondhjemites[38]. Hence the loci of TTG melt generations were likely confined within the reworked silicified metabasalts carrying relatively low -silica content (black cross in Fig. 1B).

ORIGIN OF THE HEAVY SI ISOTOPIC SIGNATURE OF GMS.

Two major mechanisms have been invoked to explain the origin of K-rich GMS melts: (1) melting of older TTG gneisses[30,35]; (2) partial melting of enriched tholeiites[33] or medium-to-high-K basalts[39]. At first sight the high $\delta^{30}Si$ values of most GMSs (close to the TTG range) appear to be straightforward evidence in favour of their derivation from the melting of a TTG-rich protocrust. However, the relationship between pluton ages, their $\delta^{30}Si$ values, and Eu anomalies (Fig. 3) indicate that a clear distinction should be made between most of the oldest (≥3.11Ga) K-rich granites (Dalmein, Nelspruit, Piggs Peak, Salisbury Kop plutons), which bear very similar $\delta^{30}Si$, Eu/Eu* (>0.7) and Sr/Y (13-53, supplementary Fig. 2B) to TTGs,

and the younger (≈3.1-2.69Ga) GMS intrusions, which have slightly lighter δ^{30}Si signatures, significantly more negative Eu anomalies (<0.6) and lower Sr/Y (<10, supplementary Fig. 2B). Partial melting of a TTG-like source should be characterized by large proportions (>45wt%)[35] of plagioclase left in the restitic assemblages after the extraction of the felsic melts. Older GMSs with small or no Eu anomalies are inconsistent with such a plagioclase-rich residual assemblages. For this reason we speculate that these older K-rich granites kept tapping a heavy δ^{30}Si silicified metabasalt-like reservoir, but with overall higher K_2O/Na_2O ratios coupled with larger silica contents (which promotes K/Na increases in the melt[38]) than our proposed source for the trondhjemitic melts. This may explain the presence of K-rich granites in the >3.2Ga record[30]. Conversely, the younger K-rich granitoids likely record melting of a pre-existing TTG-like felsic crust. Because micas are known to be enriched in ^{28}Si with respect to feldspar with a $\Delta^{30}Si_{Mica\text{-}feldspar}$ of about -0.3‰ in a tonalitic composition[21] and the $\Delta^{30}Si_{Plagioclase\text{-}melt}$ is positive at circa +0.1‰[9], the trend to lighter δ^{30}Si signatures of these younger GMSs may just reflect mineral-melt segregation at the TTG melting sites, if melt fertility was controlled by mica abundance and balanced with restitic feldspars.

GLOBAL ARCHAEAN AND HADEAN IMPLICATIONS.

Our observations suggest that the intense supracrustal silicifications of mafic lavas ubiquitous on the Archean seafloor prior to 3.0 Ga played a major role in the composition of granitoids that formed the early felsic continental crust on Earth. This unravels the importance of feedbacks between the surface and deep Earth processes during the Paleoarchean. Accordingly we infer a possible genetic link between the reworking at depth of these silicified mafic protoliths and the extensive Si-enrichment of the Kaapvaal subcontinental lithospheric mantle about 3.3Ga ago[40]. Although such a similar seawater-

209 derived silicon recycling to depth has been detected on a much smaller isotopic scale on
210 some Phanerozoic andesites[11] the effect on the Archean TTGs is an order of magnitude
211 larger reflecting the "non-actualistic" recurrent silicification of Archean supracrustal rocks
212 which fully contrasts with the scarcity of silicification at the modern altered seafloors. This
213 Archean alteration is accompanied by large major and trace element redistributions[29] many
214 of which being different from the element changes observed during the seawater
215 percolation into the modern oceanic crust. The substantial lowering of Lu/Hf ratio in the
216 silicified basalts appears as its archetype of this non-actualistic alteration (Fig. 2) because it
217 strongly contrasts with the lack of Lu/Hf disturbance by modern sea floor alteration
218 processes[41].

219 A caveat to our findings is that all data come from the Kaapvaal craton in southern
220 Africa, and hence there could be a geographical bias. However, the various constituent
221 layers (Qz-feldspar-, amphibole-, mica-rich layers) of the 3.8Ga tonalitic Amîtsoq Gneiss
222 (Isua, West Greenland) exhibit similar heavy δ^{30}Si values[21] (Fig.3). Trail et al.[42] have recently
223 proposed that Archean-Hadean detrital zircons extracted from the Jack Hills
224 metaconglomerate (Yilgarn craton, Western Australia) bear seawater-derived Si isotopic
225 signatures. Zircons are enriched in ^{28}Si relative to whole-rock[43], with a $\Delta^{30}Si_{WR\text{-}zircon}$ of about
226 +0.35‰ for tonalitic felsic systems[42]. Applying this fractionation factor to the Jack Hills δ^{30}Si
227 database of detrital zircons[42], we can evaluate the δ^{30}Si of felsic whole-rocks from which
228 they were eroded. Most are in the range of the Barberton and Isua TTGs (Fig.3), revealing
229 that most felsic rocks since the early Archean (and possibly the Hadean) might carry similar
230 proportions of seawater-derived silicon. This highlights the likely global significance of
231 reworked silicified seafloor protoliths as an essential element to generate the primordial
232 felsic nuclei of continental crust.

*Corresponding author

By linking the primeval growth of silicic crust to the evolution of seawater-mafic rock interactions on the early Earth, we implicitly address the question of why granitoid rocks are rare or absent on other terrestrial planets, in particular in the Martian crust which is mostly basaltic (~50wt% SiO_2) with few subalkaline rock-types perhaps petrographically reminiscent of TTGs[44]. With the rapid disappearance of an early ocean somewhere around 4.1-3.7 Ga years ago[45,46], Mars lacked its surficial Si-saturated water reservoir that would have been able to intensively interact with its basaltic crust for a long time period. The absence or the restricted scale of such interactions prevented the accumulation of Si-rich metabasalts and their transport to depth that would have been essential to trigger the formation of a thick TTG-like protocrust.

Methods

Silicon isotopes. Silicon was concentrated from 5 mg of powdered sample digested with 0.2g analytical grade NaOH into carbon SIGRADUR® crucibles at 730°C for 10 min in a muffle furnace. The fusion beads were dissolved in 50ml bi-distilled 0.01M HNO_3 to obtain a Si stock solution sufficiently dilute to avoid silicic acid polymerization. The acidified solution at pH~2 was recommended[51] for the complete dissolution of Fe-oxyhydroxides and a quantitative elution yield without Si isotopic fractionation during the following purification step. The sample solution was eluted on 1.8 mL BioRad AG 50W-X12 (200-400 mesh, hydrogen form) cation exchange resin, conditioned with the different HCl and HNO_3 pre-cleaning and Milli-Q water rinse steps[52]. 3 mL of ~60 µg Si were loaded on the column and eluted with 2 mL Milli-Q water. Although the speciation of dissolved Si in water is pH dependent, it occurs as neutral or anionic species at low to neutral pH and thus is not retained by the resin whereas cationic matrix elements are efficiently retained. The final solution of ~10 ppm Si was

directly acidified to 0.14M HNO_3 for isotope analyses. The reference standards were prepared according to this same method in parallel with the specimens. Quantitative recovery of Si for the global method was 99 ± 4 %. The full chemical preparation has been replicated 3 or 4 times on all samples starting from the rock powders to check the reproducibility of the chemical procedure.

Si isotopic compositions were measured using Nu Plasma II MC-ICP-MS in dry plasma mode using the CETAC Aridus II desolvator at the Université Libre de Bruxelles (ULB, Brussels), following our published methodologies[53]. The sample introduction system was equipped with a CETAC C-Flow PFA concentric nebulizer with an uptake rate of 100 µL/min. The membrane and spray chamber of desolvator were cleaned with 10% v/v warm (70°C) HNO_3 and dried with isopropanol on argon gas flush to eliminate any residues that may compromise the analyses by memory effect and/or high background. The instrumental mass bias and drift were corrected both with external Mg doping applying the exponential mass bias law and with the standard-sample bracketing method[54]. To resolve all molecular interferences ($^{28}SiH^+$,$^{14}N^{2+}$ and $^{14}N^{16}O^+$), the measurements were performed in Pseudo-High Resolution on the interference-free lower mass side of the plateau of flat top peaks setting with an offset next to mid-slope. A single analysis consists in 3 blocks of 20 runs with 5 second integration time by run on each Si and Mg isotope separated by 2 seconds to allow the parameter switch in dynamic mode. The average within-run reproducibility was 0.14‰ (2SD). Typical Si sensitivity was ~20 V/ppm with 500-1000 signal/blank ratio which represents a 4-6 fold improvement compared to our earlier published conditions (125<signal/blank<175)[53]. The Mg doping concentration was adjusted to 0.4 ppm Mg for 1 ppm Si to have the Si/Mg voltage ratio close to 1.

*Corresponding author

Nine specimens for which we replicated the total chemical procedure four times have been analysed with two different mass spectrometers. Two powder solutions were measured 3 times each with the ULB Nu instrument following the aforementioned procedure. The remaining two powder solutions were run 3 times each with a Neptune MC-ICPMS at the Pôle Spectrométrie Ocean (Brest), using an APEX desolvation unit and a medium mass resolution mode following a methodology described in Ref. 14. The gap ($\Delta_{\text{Nu-Neptune}}$) between the mean of both groups of measurements varies between 0.02‰ and 0.08‰ with a mean of 0.04‰ (Supplementary Table 4). This provides an important analytical validation of our in-house determinations and demonstrates the optimal character of six repetitions on two powder aliquots. Hence, we could routinely use the two standard error of the mean ($2\sigma_{\bar{X}}$) of six total replicates (two duplicates of three powder aliquots) as a correct estimate of how far the sample mean of the data is likely to be from the true population mean with a probability of 95%. This is the external error associated to each measurement listed in supplementary table 2. On average, it is ±0.03‰ and ±0.05‰ for δ^{29}Si and δ^{30}Si respectively.

Data are reported as δ values in per mil relative to the international NBS-28 silica standard. Several external standards (GA granite, BHVO-2 basalt and diatomite) were regularly measured during each analytical session. The long-term reproducibilities for δ^{30}Si obtained on these three standards and given by 2 standard deviation (2SD) over two years measurements were of 0.16‰ (n=76), 0.18‰ (n=37), 0.19‰(n=88), respectively. Our results gave a mean δ^{30}Si value of -0.24±0.02‰ ($2\sigma_{\bar{X}}$, n=76) for GA, -0.29±0.03‰ ($2\sigma_{\bar{X}}$, n=37) for BHVO-2 and +1.26±0.02‰ ($2\sigma_{\bar{X}}$ n=88) for Diatomite. They are all in very good agreement within uncertainties with the previous measurements the reference of which are given in the Supplementary Table 2. All granitoid samples and the standards analysed in this study

*Corresponding author

define, within error, a good terrestrial mass-dependent fractionation law ($\delta^{29}Si=0.5095x\delta^{30}Si$, Supplementary Fig. 4A,B) which is consistent with equilibrium (slope $0.5178\delta^{30}Si$) or kinetic (slope $0.5092\delta^{30}Si$) mass-dependent fractionations.

Major and trace element compositions for specimens 99/xxx are all from Ref. 24. Major element and trace element compositions for specimens BAR 1 to 10 were obtained by X-ray fluorescence (XRF) (major elements) and ICP-MS (trace elements) at the University of Mainz, Germany, and followed standard procedures[55]. Data for SW-1 and MG18/MG35 have been reported in ref. 56 and 57, respectively. For BAR11-16, SINC1, and SINC2, major element contents were determined as reported in ref. 57, while trace elements where analysed by ACME laboratories in Vancouver, Canada, using ICP-MS following lithium borate fusion. The relative total errors for the rare earth elements are usually around 5% while those for the high field strength elements and the large ion lithophile elements span 5 to 15%. These unpublished results are compiled in supplementary Table 5.

REFERENCES

1. Belousova, E.A., Kostitsyn, Y.A., Griffin, W.L., Begg, G.C., O'Reilly, S.Y. et al. The growth of the continental crust: constraints from zircon Hf-isotope data. *Lithos* **119**, 457-466 (2010).
2. Dhuime, B., Hawkesworth, C.J., Delavault, H. & Cawood, P.A. Continental growth seen through the sedimentary record. *Sediment. Geol.* **357**, 16-32 (2017).
3. Pujol, M., Marty, B., Burgess, R., Turner, G. & Philippot, P. Argon isotopic composition of Archaean atmosphere probes early Earth geodynamics. *Nature* **498**, 87-90 (2013).

*Corresponding author

4. Rosas J.C. & Korenaga J. Rapid crustal growth and efficient crustal recycling in the early Earth: implications for Hadean and Archean geodynamics. *Earth Planet. Sci. Lett.* **494**, 42–49. (2018).

5. Taylor, S.R. Abundance of chemical elements in the continental crust: a new table. *Geochim. Cosmochim. Acta* **28**, 1273-1285 (1964).

6. Savage, P.S., Armytage, R.M.G., Georg, R.B. & Halliday, A.E. High temperature silicon isotope geochemistry. *Lithos* **190-191**, 500-519 (2014).

7. Pringle, E.A., Moynier, F., Savage, P.S., Jackson, M.G., Moreira, M. et al. Silicon isotopes reveal recycled altered oceanic crust in the mantle sources of ocean island basalts. *Geochim. Cosmochim. Acta* **189**, 282–295 (2016).

8. Savage, P.S., Georg, R.B., Armytage, R.M.G., Williams, H.M. & Halliday, A.N. Silicon isotope homogeneity in the mantle. *Earth Planet. Sci. Lett.* **295**,139–146 (2010).

9. Savage, P.S., Georg, R.B., Williams, H.M., Burton, K.W. & Halliday, A.N. Silicon isotope fractionation during magmatic differentiation. *Geochim. Cosmochim. Acta* **75**, 6124–6139 (2011).

10. Savage, P.S., Georg, R.B., Williams, H.M., Turner, S., Halliday, A.N. et al. The silicon isotope composition of granites. *Geochim. Cosmochim. Acta* **92**, 184–202 (2012).

11. Poitrasson F. & Zambardi T. An Earth–Moon silicon isotope model to track silicic magma origins. *Geochim. Cosmochim. Acta* **167**, 301–312 (2015).

12. Frings, P.J., Clymans, W., Fontorbe, G., De La Rocha C., L. & Conley, D.J. The continental Si cycle and its impact on the ocean Si isotope budget. *Chem. Geol.* **425**, 12–36 (2016).

*Corresponding author

13. Kleine, B.I., Stefánsson A., Halldórsson S.A., Whitehouse, M.J. & Jónasson, K. Silicon and oxygen isotopes unravel quartz formation processes in the Icelandic crust. *Geochem. Persp. Let.* **7**, 5-11 (2018).

14. Bayon, G., Delvigne, C., Ponzevera, E., Borges, A., Darchambeau, F., et al. The silicon isotopic composition of fine-grained river sediments and its relation to climate and lithology. *Geochim. Cosmochim. Acta* **229**, 147–161 (2018).

15. Chakrabarti, R., Knoll, A.H., Jacobsen, S.B. & Fischer, W.W. Si isotope variability in Proterozoic cherts. *Geochim. Cosmochim. Acta* **91**, 187–201 (2012).

16. Zheng X.-Y., Beard, B.L., Reddy, T.R., Roden, E.E. & Johnson C.M. Abiologic silicon isotope fractionation between aqueous Si and Fe(III)–Si gel in simulated Archean seawater: Implications for Si isotope records in Precambrian sedimentary rocks. *Geochim. Cosmochim. Acta* **187**, 102–122 (2016).

17. Delvigne C., Cardinal D., Hofmann A. & André L. Stratigraphic changes of Ge/Si, REE+Y and silicon isotopes as insights into the deposition of a Mesoarchaean banded iron formation. *Earth Planet. Sci. Lett.* **355–356**, 109–118 (2012).

18. Robert F. & Chaussidon M. A palaeotemperature curve for the Precambrian oceans based on silicon isotopes in cherts. *Nature* **443**, 969–972 (2006).

19. Marin-Carbonne J., Robert F. & Chaussidon M. The silicon and oxygen isotope compositions of Precambrian cherts: a record of oceanic paleo-temperatures? *Precambr. Res.* **247**, 223–234 (2014).

20. Abraham K., Hofmann A., Foley S. F., Cardinal D., Harris C., et al. Coupled silicon-oxygen isotope fractionation traces Archaean silicification. *Earth Planet. Sci. Lett.* **301**, 222–230 (2011).

*Corresponding author

21. André, L., Cardinal, D., Alleman, L.Y. & Moorbath, S. Silicon isotopes in ∼3.8 Ga West Greenland rocks as clues to the Eoarchaean supracrustal Si cycle. *Earth Planet. Sci. Lett.* **245**, 162-173 (2006).

22. Zambardi T., Lundstrom CC, Li X. & McCurry M. Fe and Si isotope variations at Cedar Butte volcano; Insight into magmatic differentiation. *Earth Planet. Sci. Lett.* **405**, 169–179 (2014).

23. Rapp, R.P. & Watson, E.B. Dehydratation melting of metabasalt at 8–32 kbar: implications for continental growth and crust–mantle recycling. *J. Petrol.* **36**, 891–931 (1995).

24. Kleinhanns, I.C., Kramers, J.D. & Kamber, B.S. Importance of water for Archaean granitoid petrology: a comparative study of TTG and potassic granitoids from Barberton Mountain Land, South Africa. *Contrib. Mineral. Petrol.* **145**, 377–389 (2003).

25. Méheut M. & Schauble E.A. Silicon isotope fractionation in silicate minerals: insights from first-principles models of phyllosilicates, albite and pyrope. *Geochim. Cosmochim. Acta* **134**, 137–154 (2014).

26. Yu H.-M., Li Y.-H., Gao Y.-J. Huang J. & Huang F. Silicon isotopic compositions of altered oceanic crust: Implications for Si isotope heterogeneity in the mantle. *Chem. Geol.* **479**, 1-9 (2018).

27. Richter F. M., Watson E. B., Mendybaev R., Dauphas N., Georg B., et al. Isotopic fractionation of the major elements of molten basalt by chemical and thermal diffusion. *Geochim. Cosmochim. Acta* **73**, 4250–4263 (2009).

*Corresponding author

391 28. Gajos N.A., Lundstrom, C.C. & Taylor A.H. Spatially controlled Fe and Si isotope
392 variations: an alternative view on the formation of the Torres del Paine pluton.
393 *Contrib. Mineral. Petrol.* **171**: 93. https://doi.org/10.1007/s00410-016-1302-4 (2016).
394 29. Hofmann, A. & Harris, C. Silica alteration zones in the Barberton Greenstone Belt: a
395 window into subseafloor processes 3.5-3.3 Ga ago. *Chem. Geol.* **257**, 221-239 (2008).
396 30. Agangi, A. Hofmann, A. & Elburg M.A. A review of Palaeoarchaean felsic volcanism in
397 the eastern Kaapvaal craton: Linking plutonic and volcanic records. *Geosci. Front.* **9**,
398 667-688 (2018).
399 31. DePaolo, D.J. Trace element and isotopic effects of combined wallrock
400 assimilation and fractional crystallization. *Earth Planet. Sci. Lett.* **53**, 189–202 (1981).
401 32. Smithies R.H., Ivanica T.J., Lowrey J.R., Morris P.A., Barnes S.J., et al. Two distinct
402 origins for Archean greenstone belts. *Earth Planet. Sci. Lett.* **487**, 106–116 (2018).
403 33. Johnson, T.E., Brown, M., Gardiner, N.J., Kirkland, C.L. & Smithies, R.H. Earth's first
404 stable continents did not form by subduction. *Nature* **543**, 239–242 (2017).
405 34. Blichert-Toft, J. & Albarède, F. Hafnium isotopes in Jack Hills zircons and the
406 formation of the Hadean crust. *Earth Planet. Sci. Lett.* **265**, 686–702 (2008).
407 35. Gardiner, N.J., Johnson, T.E., Kirkland, C.L. & Smithies, R.H. Melting controls on the
408 lutetium–hafnium evolution of Archaean crust. *Precam. Res.* **305**, 479-488 (2018).
409 36. Gilbert M.C., Helz R.T., Popp R.K. & Spear F.S. Experimental studies of amphibole
410 stability. *Rev. Mineral.* **9B**, 229-353 (1982).
411 37. Foley S.F., Buhre S. & Jacob D.E. Evolution of the Archaean crust by delamination and
412 shallow subduction. *Nature* **421**, 249-252 (2003).
413 38. Patiño Douce A.E. & Beard J.S. Dehydration-melting of biotite gneiss and quartz
414 amphibolite from 3 to 15 kbar. *J. Petrol.* **36**, 707-738 (1995).

*Corresponding author

415 39. Sisson, T.W., Ratajeski K., Hankins W.B. & Glazner A.F. Voluminous granitic magmas
416 from common basaltic sources. *Contrib. Mineral. Petrol.* **148**, 635-661 (2005).
417 40. Van der Meer Q.H.A., Klaver M., Reisberg L., Riches A.J.V. & Davies G.R. Preservation
418 of an Archaean whole rock Re-Os isochron for the Venetia lithospheric mantle:
419 Evidence for rapid crustal recycling and lithosphere stabilisation at 3.3Ga. *Geochim.*
420 *Cosmochim. Acta* **216**, 242–263 (2017).
421 41. Thompson, P.M.E., Kempton, P.D. & Kerr A.C. Evaluation of the effects of alteration
422 and leaching on Sm–Nd and Lu–Hf systematics in submarine mafic rocks. *Lithos* **104**,
423 164-176 (2008).
424 42. Trail D., Boehnke P., Savage, P. S., Liu M.-C., Miller M.L. et al. Origin and significance
425 of Si and O isotope heterogeneities in Phanerozoic, Archean, and Hadean zircon.
426 *Proc. Natl. Acad. Sci. USA* **115**(41),10287-10292 (2018).
427 43. Qin T., Wu F., Wu Z.Q. & Huang F. First-principles calculations of equilibrium
428 fractionation of O- and Si isotopes in quartz, albite, anorthite, and zircon. *Contrib.*
429 *Mineral. Petrol.* **171**, 91 (2016).
430 44. Sautter M.J., Toplis R.C., Cousin A, Fabre C., Gasnault O. et al. In situ evidence for
431 continental crust on early Mars. *Nature Geosci*. **8**, 605-609 (2015).
432 45. Fawdon P., Gupta S., Davis J.M., Warner N.H., Adler J.B., et al. The Hypanis Valles
433 delta: The last highstand of a sea on early Mars? Earth Planet. Sci. Lett. **500**, 225-241
434 (2018).
435 46. Rickman, H. Błęcka M.I., Gurgurewicz J., Jørgensen U.G., Słaby E., Szutowicz S. &
436 Zalewska N. Water in the history of Mars: An assessment. *Planet. Space Sci.* **166,** 70-
437 89 (2019).

*Corresponding author

47. Savage, P.S., Georg, R.B., Williams, H.M. & Halliday, A.N. Silicon isotopes in granulite xenoliths: insights into isotopic fractionation during igneous processes and the composition of the deep continental crust. *Earth Planet. Sci. Lett.* **365**, 221–231 (2013).

48. Geilert, S., Vroon, P. Z. & van Bergen, M. J. Silicon isotopes and trace elements in chert record early Archean basin evolution. *Chem. Geol.* **386**, 133–142 (2014).

49. Gale A., Dalton C.A., Langmuir C.H., Su Y. & Schilling J.-G. The mean composition of ocean ridge basalts. Geochim. Geophy. Geosy. 14 –doi:10.1029/2012GC004334 (2013).

50. Furnes H., Robins, B. & De Wit M.J. Geochemistry and petrology of lavas in the upper Onverwacht suite, Barberton Mountain Land, South Africa. S. Afr. J. Geol. **115,** 171-210 (2012).

METHODS REFERENCES

51. Fitoussi, C., Bourdon, B., Kleine, T., Oberli, F. & Reynolds, B.C. Si isotope systematics of meteorites and terrestrial peridotites: implications for Mg/Si fractionation in the solar nebula and for Si in the Earth's core. *Earth Planet. Sci. Lett.* **287**, 77–85 (2009).

52. Georg, R.B., Reynolds, B.C., Frank, M. & Halliday, A.N. New sample preparation techniques for the determination of Si isotopic compositions using MC-ICPMS. *Chem. Geol.* **235**, 95–104 (2006).

53. Abraham, K., Opfergelt, S., Fripiat, F., Cavagna, A.-J., de Jong, J.T.M., et al. δ^{30}Si and δ^{29}Si determinations on USGS BHVO-1 and BHVO-2 reference materials with a new configuration on a Nu Plasma Multi-Collector ICP-MS. *Geostand. Geoanal. Res.* **32**, 193–202 (2008).

*Corresponding author

461 54. Cardinal, D., Alleman, L.Y., De Jong, J., Ziegler, K. & André, L. Isotopic composition of
462 silicon measured by multicollector plasma source mass spectrometry in dry plasma
463 mode. *J. of Anal. At. Spectrom.* **18**, 213–218 (2003).
464 55. Nehring, F., Jacob, D.E., Barth, M.G., Foley, S.F. Laser-ablation ICP-MS analysis of
465 siliceous rock glasses fused on an iridium strip heater using MgO dilution. *Microchim.*
466 *Acta* **160**, 153-163 (2008).
467 56. Hofmann, A., Kröner, A., Xie, H., Hegner, E., Belyanin, G., et al. The Nhlangano gneiss
468 dome in south-west Swaziland–a record of crustal destabilization of the eastern
469 Kaapvaal craton in the Neoarchaean. Precambr. Res. **258**, 109-132 (2015).
470 57. Dlamini N., Hofmann, A., Belyanin, G., Xie, H., Kröner, A., et al. Supracrustal gneisses
471 in southern Swaziland: a basalt-sandstone assemblage of the upper Mozaan Group
472 deformed in the Neoarchaean. South Afr. J. of Geology **120**, 477-498 (2017).

473

474 **Corresponding author**

475 Correspondence and requests for materials should be addresses to L.A.
476 (lucandre@africamuseum.be)

477 **Acknowledgements**

478 We acknowledge G. Ponzevera and G.Bayon (IFREMER, Brest, France) for their careful
479 help with the duplicate Neptune MC-ICP-MS analyses of a few specimens.

480 **Author contributions**

481 The project was conceived by L.A. and S.F. Si isotope analyses were performed by L.M.,
482 L.A., and K.A. and interpreted by L.A. with S.F., A.H. and K.A. The manuscript was written
483 chiefly by L.A. with S.F. and A.H. Fieldwork and petrological inputs were provided by
484 K.A., L.K. and A.H.

*Corresponding author

485 **Competing financial interests**

486 The authors declare no competing financial interests.

487

*Corresponding author

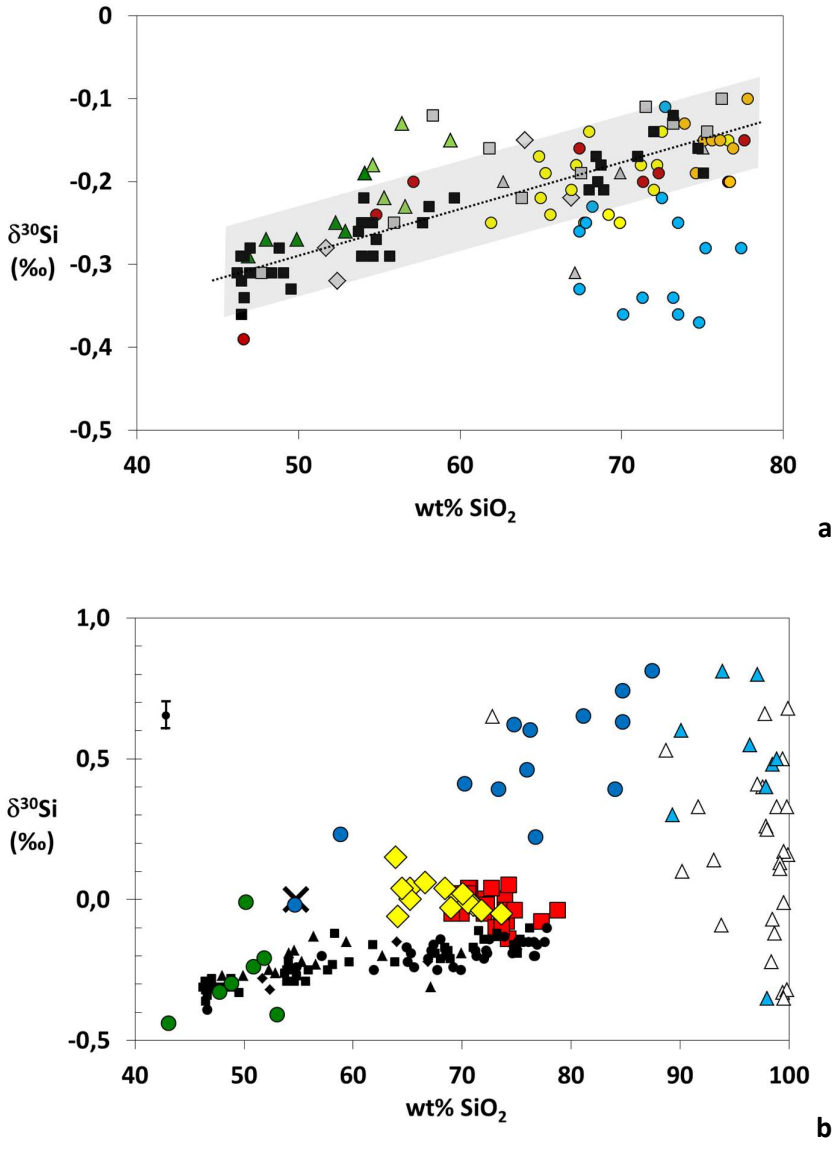

Fig. 1 Bulk rock silicon isotopic compositions plotted against their SiO_2 contents. a. The dotted line marks the linear "igneous array" of equation [δ^{30}Si (‰) =0.0056 x SiO_2 (wt%) - 0.567] defined by the differentiation trends of Afar and Iceland[9] (black squares). The grey domain is a $2\sigma_{\bar{X}}$ uncertainty of ±0.05‰ around that trend line[9]. Most other terrestrial igneous rocks plot within this domain: the Cedar Butte volcano differentiation trend from the Snake River[22] (grey squares); the Finland granophyre from the Duluth complex[22] (grey triangles); the Torres del Paine differentiation trend[28] (brown circles); aluminous I-type

498 granites[10,11] (yellow circles); peralkaline A-type granites[10,11] (orange circles); mafic and felsic
499 melts from the granulitic McBride xenoliths[47] (grey diamonds); basalts, gabbro, diorite (dark
500 green triangles) and some calk-alkaline andesites[11] (light green triangles). Peraluminous S-
501 type granites[10,11] (blue circles) constitute a prominent exception, deviating markedly
502 towards low δ^{30}Si. **b.** Silicon isotopic compositions of bulk Barberton TTG (yellow diamonds)
503 and GMS (red squares) granitoid rocks consistently heavier than rocks of the terrestrial
504 "igneous array" (the small black symbols figure all rocks which fit the igneous array in Fig 1a).
505 TTGs plot just to the right of the array defined by unsilicified (green circles) and silicified
506 (blue circles) metabasalts and intercalated cherts (blue triangles) from the Onverwacht
507 Group[20]. Other cherts from the Buck Reef Chert of Barberton (white triangles)[48] are plotted
508 for comparison. The error bar represents the average $2\sigma_{\bar{X}}$ error (0.05‰) on δ^{30}Si (Methods).
509 The oblique cross represents the composition of the TTG proposed source.

510

511

512

*Corresponding author

513

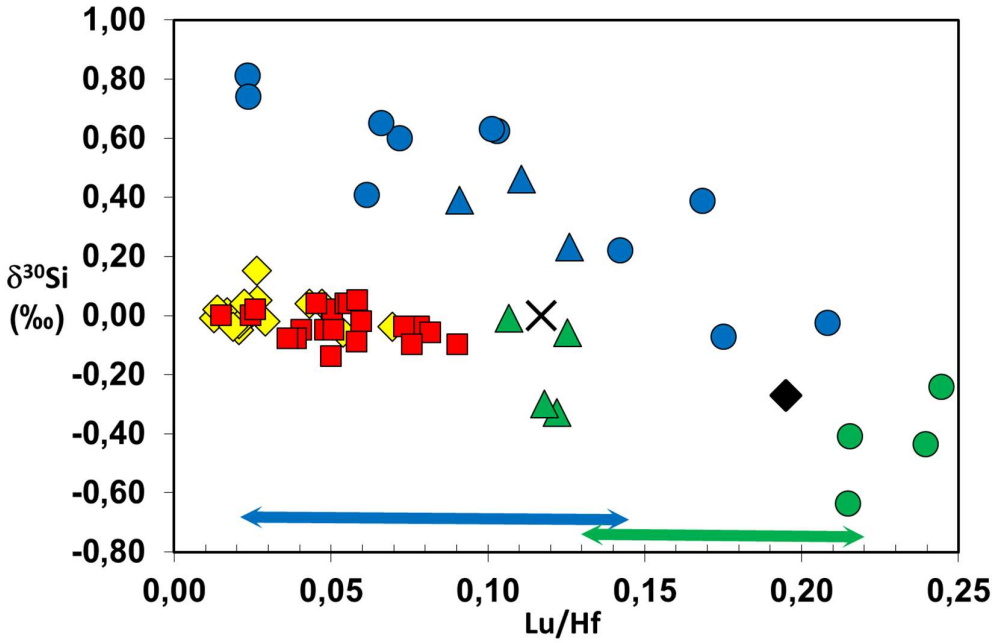

514

515 **Fig. 2 δ^{30}Si *versus* Lu/Hf diagram.** Lu/Hf data for Theespruit (triangles) and Hooggenoeg-
516 Kromberg (circles) metabasalts are taken from reference 29. The N-MORB (black diamond)
517 Lu/Hf and δ^{30}Si are from references 49 and 6 respectively. The Lu/Hf were disturbed in all
518 silicified (blue symbols) and unsilicified (green symbols) metabasalts, as a consequence of
519 the geochemical redistributions operated by their respective alterations[29] because they all
520 keep similar N-MORB La/Nb and Th/Nb ratios (Supplementary Table 3). This is confirmed by
521 the range of Lu/Hf ratios (± 1SD) observed from another large database of silicified
522 (SiO_2>60wt%, Lu/Hf=0.084±0.062, n=16, blue arrow) and unsilicified (SiO_2<60wt%,
523 Lu/Hf=0.174±0.045, n=81, green arrow) Onverwacht basalts[50]. The low Lu/Hf of the
524 proposed TTG source (oblique cross) fits the low Lu/Hf features of BGB TTGs and GMSs
525 (Symbols as in fig. 1B).

526

*Corresponding author

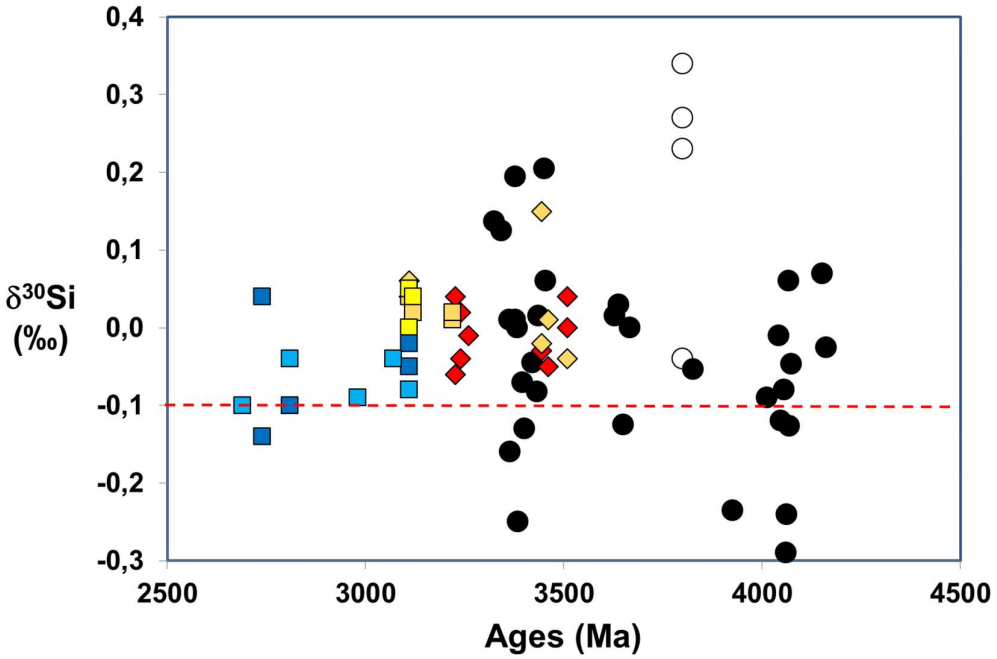

527

528

529 **Fig. 3 Hadean-Archean δ^{30}Si granitoid signatures.** This δ^{30}Si *vs* age diagram compares TTG
530 (diamonds) and GMS (squares) data of this study to compositionally different layers from the
531 Amîtsoq gneiss[21] (open circles) and computed δ^{30}Si values of pre-3.3Ga felsic rocks (filled
532 circles) from which detrital Jack Hills zircons[42] have been eroded. Note that the error bars on
533 SIMS zircon δ^{30}Si values is larger (±0.2‰)[42] than the MC-ICP-MS δ^{30}Si values (±0.05‰). The
534 colour code for TTG and GSM refers to their Eu anomaly: red, Eu/Eu*>1; orange,
535 0.8<Eu/Eu*<1; yellow, 0.6<Eu/Eu*<0.8; dark blue, 0.4<Eu/Eu*<0.6; light blue, Eu/Eu*<0.4.
536 The dashed red line represents the upper limit (~-0.1‰) of the igneous array at 75 wt% SiO_2.
537 All rocks above this threshold are regarded to carry a significant proportion of seawater-
538 derived Si in their protoliths.

539

540

*Corresponding author

Supplementary figures and tables

of the paper entitled "ORIGIN OF EARLY CONTINENTAL CRUST BY REWORKING SILICIFIED METABASALTS" by André et al.

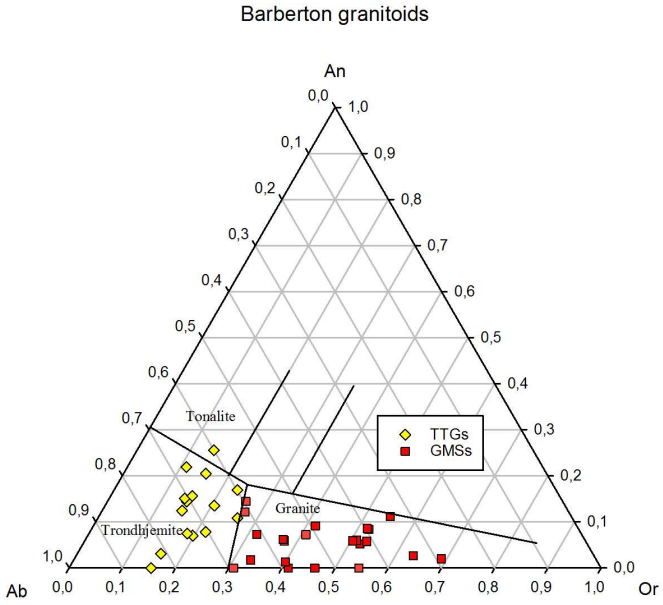

Supplementary figure 1: Normative Ab-An-Or compositions of the analysed whole-rocks. The three granites which are plotted very close to the boundary between the trondhjemitic and granitic fields correspond to two specimens from the Dalmein pluton (Bar-10 & 99/108) and one sample from the Nelspruit pluton (99/118).

*Corresponding author

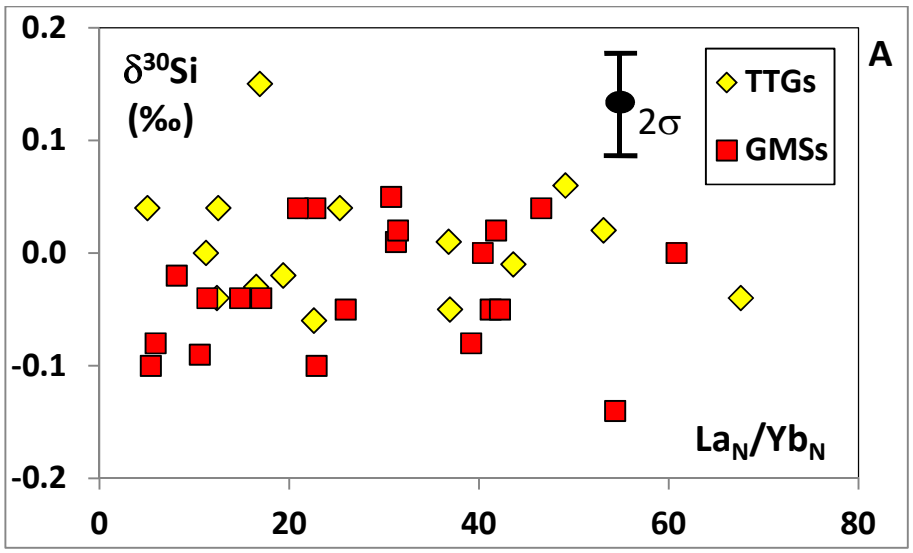

Supplementary figure 2A: δ^{30}Si-La_N/Yb_N diagram for the TTGs and GMSs.

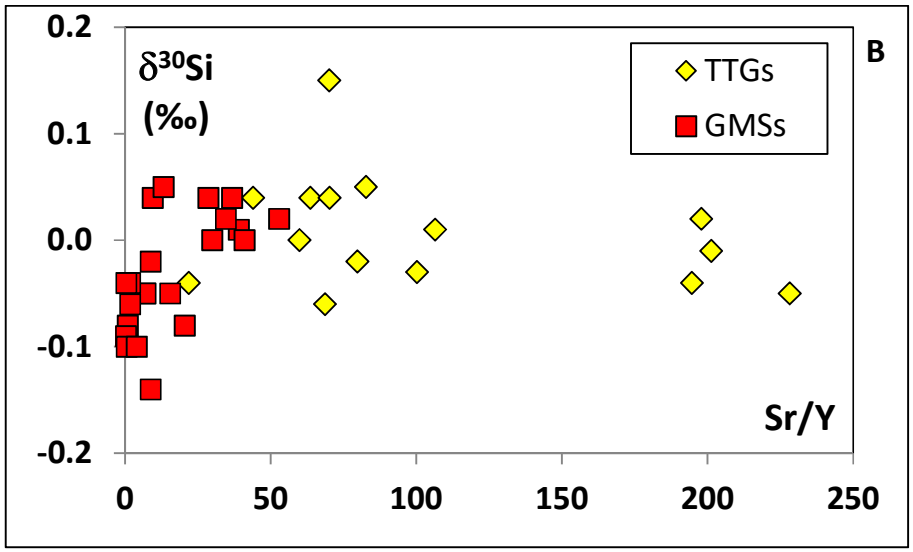

Supplementary figure 2B: δ^{30}Si-Sr/Y diagram for the TTGs and GMSs.

*Corresponding author

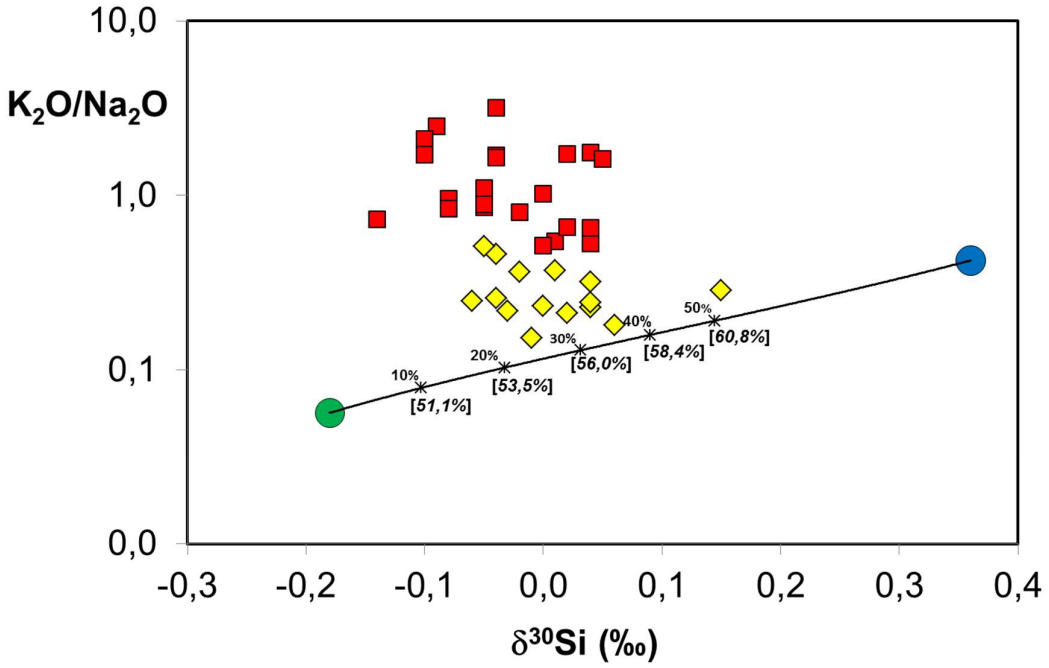

Supplementary Fig. 3 K_2O/Na_2O versus $\delta^{30}Si$ plot for the TTGs (yellow diamonds) and GMSs (red squares). Models are calculated for mixtures between the Theespruit unsilicified metabasalts average (green circle) and the Theespruit silicified metabasalt average (blue circle). Ticks and numbers next to the mixing curve indicate the proportion of silicified material in the mixtures (one tick every 10%). Figures within brackets close to the curve give the silica contents (in wt%) of the mixtures. Considering that K_2O/Na_2O should increase slightly in partial melts relative to their source-rocks[33,38], the mixtures including about 20-35% of Theespruit-like silicified metabasalts would account for both typical Barberton K_2O/Na_2O and $\delta^{30}Si$ features. More silicified metabasalts in the source might cause much larger K_2O/Na_2O in the produced melt because: (1) the silicified metabasalts have higher K_2O/Na_2O than their unsilicified counterparts (Supplementary Table 3) and (2) larger quantities of silica in the source ($\geq$ 60wt%) induce granitic like melts with higher K_2O/Na_2O[38]. Such high silicified sources might be the protoliths for the older GMS characterised by heavier $\delta^{30}Si$ (>0‰).

*Corresponding author

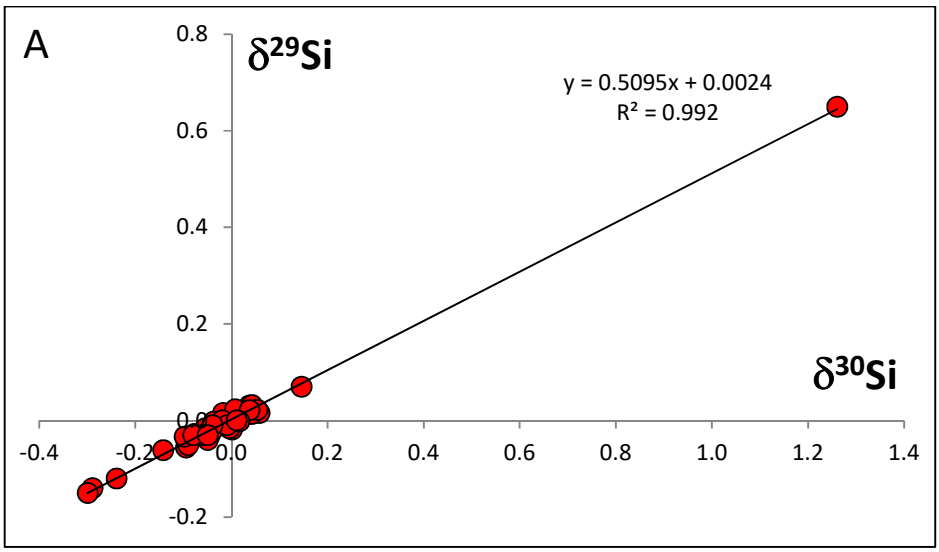

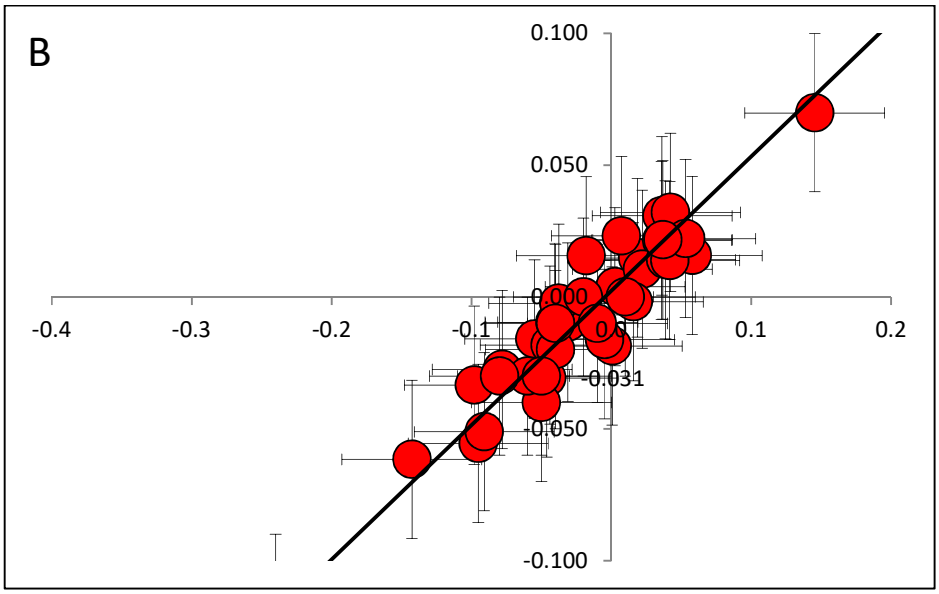

Supplementary figure 4: A. Three isotope plot for the granitoid rocks and the GA, BHVO-1, BHVO-2 and diatomite standards. They fit a line of $\delta^{29}Si=0.5095x\delta^{30}Si$; B. Enlargement of the granitoid specimens showing that they all fit this line within uncertainties (±0.03‰ and ±0.05‰ for $\delta^{29}Si$ and $\delta^{30}Si$, respectively).

*Corresponding author

597

598

599 Supplementary Table 1: Geographic coordinates of the analysed
600 specimens

Sample	Pluton	Latitude	Longitude
99/109	Steynsdorp	26°10'33'' S	030°59'51'' E
99/122	Steynsdorp	26°11'00'' S	030°40'34'' E
Bar-6	Steynsdorp	25°09`12.9``S	30°57`20.1``
99/120	Stolzburg	26°01'27'' S	030°45'41'' E
Bar-2	Stolzburg	26°01`27.9``S	30°45`41.7``
99/107	Theespruit	26°02'00'' S	030°50'31'' E
99/121	Theespruit	26°03'00'' S	030°51'46'' E
Bar-3	Theespruit	26°01`25.0``S	30°48`07.3``
Bar-5	Badplaas	25°57`43.9``S	30°35`24.4``
99/106	Nelshoogte	25°51'06'' S	030°41'59'' E
Bar-9	Nelshoogte	25°53`29.0``S	30°37`24.2``
Bar-8	Kaap Valley	25°44`06.3``S	31°04`10.1``
Bar-10	Dalmein	26°05`24.1``S	30°56`16.9``
99/108	Dalmein	26°04'54'' S	030°55'58'' E
99/118	Nelspruit	25°29'30'' S	031°11'00'' E
99/110	Nelspruit	25°33'56'' S	030°58'14'' E
99/112	Nelspruit	25°31'20'' S	031°19'53'' E
99/119	Nelspruit	25°23'34'' S	030°58'52'' E
BAR11	Nelspruit	25°27'29.0'' S	31°01'01.5''
BAR12	Mpageni	25°30'56.4''S	31°13'42.7''
99/111	Mpageni	25°30'41'' S	031°12'47'' E
BAR14	Piggs Peak	25°57'24.8''S	31°16'29.4''
BAR15	Piggs Peak	26°07'12.1''S	31°10'19.4''
99/115	Salisbury Kop	25°27'27'' S	031°37'34'' E
BAR13	Salisbury Kop	25°29'00.9''S	31°40'31.6''
99/117	Stentor Pluton	25°37'04'' S	031°18'23'' E
Bar-7	Stentor	25°37`02.9``S	30°18`24.3``
99/126	Mpuluzi	26°09'17'' S	030°51'36'' E
99/127	Mpuluzi	26°12'37'' S	030°35'04'' E
Bar-1	Mpuluzi	26°12`36.1`` S	30°35`03.9``
SINC1	Sinceni	26°46'07.0''S	31°29'32.1''
SINC2	Sinceni	26°50'37.9''S	31°29'37.5''
BAR16	Mbabane	26°17'42.8''S	31°08'46.0''

601

*Corresponding author

Supplementary Table 2: Si isotopic data with SiO_2 contents and key major and trace element ratios for the analysed TTGs & GMSs

	Ages (references)	Samples	Group/Lithology	n	(*) [**]	$\delta^{30}Si \pm 2\sigma_X$ ‰	$\delta^{29}Si \pm 2\sigma_X$ ‰	SiO_2	K_2O/Na_2O	Eu/Eu*	La_N/Yb_N	Lu/Hf	Sr/Y
Steynsdorp	3.51 (a,b)	99/109	TTG/Trondhjemite	3	(6)	+0.04±0.03	+0.01±0.03	65.24	0.32	1.07	5.02	0.047	43.9
		99/122	TTG/Trondhjemite	3	(6)	0.00±0.06	-0.02±0.03	65.25	0.23	1.05	11.2	0.024	59.8
		BAR-6	TTG/Trondhjemite	4	(6)+[6]	-0.04±0.07	-0.02±0.03	71.78	0.46	0.81	12.4	0.070	21.8
Stolzburg	3.46 (c)	99/120	TTG/Trondhjemite	3	(6)	+0.01±0.04	+0.02±0.04	69.78	0.37	0.94	36.8	0.017	106
		Bar-2	TTG/Trondhjemite	4	(6)+[6]	-0.05±0.07	-0.04±0.03	73.64	0.51	1.16	36.9	0.021	228
Theespruit	3.44 (a,d)	99/107	TTG/Trondhjemite	3	(6)	-0.03±0.06	-0.01±0.04	69.01	0.22	1.08	16.5	0.021	100
		99/121	TTG/Trondhjemite	3	(7)	+0.15±0.06	+0.07±0.03	63.90	0.29	0.86	16.9	0.026	70.0
		Bar-3	TTG/Trondhjemite	4	(6)+[6]	-0.02±0.05	0.00±0.03	71.09	0.37	0.88	19.4	0.029	79.7
Badplaas	3.26 (e)	Bar-5	TTG/Trondhjemite	4	(6)+[6]	-0.01±0.05	-0.01±0.03	70.59	0.15	1.29	43.6	0.013	201
Nelshoogte	3.24 (f)	99/106	TTG/Trondhjemite	3	(6)	+0.02±0.07	+0.01±0.04	70.08	0.21	1.21	53.1	0.014	198
		Bar-9	TTG/Trondhjemite	4	(6)+[6]	-0.04±0.04	-0.01±0.03	71.80	0.26	1.29	67.6	0.019	195
Kaap Valley	3.23 (a)	99/128	TTG/Trondhjemite	3	(6)	+0.04±0.06	+0.03±0.04	64.51	0.23	1.08	12.5	0.043	63.6
		Bar-8	TTG/Tonalite	4	(6)+[6]	-0.06±0.03	-0.03±0.04	64.12	0.25	1.11	22.6	0.054	68.6
Dalmein	3.20 (c)	Bar-10	GMS/Granite	4	(6)+[6]	+0.01±0.05	0.00±0.04	70.40	0.55	0.95	31.2	0.050	38.9
		99/108	GMS/Granite	3	(7)	+0.02±0.06	+0.01±0.03	69.80	0.66	0.85	31.4	0.051	34.5
Nelspruit	3.11 (a)	99/118	GMS/Granite	3	(6)	+0.00±0.06	0.00±0.03	71.95	0.52	0.74	60.8	0.015	40.9
		99/110	TTG /Trondhjemite	3	(9)	+0.06±0.06	+0.02±0.04	66.65	0.18	0.81	49.1	0.027	82.7
		99/112	TTG /Trondhjemite	3	(6)	+0.04±0.07	+0.03±0.05	68.48	0.25	0.98	25.3	0.022	70.1
		99/119	GMS/Granite	3	(6)	-0.05±0.04	-0.02±0.03	72.06	0.86	0.58	25.9	0.041	15.4
		Bar-11	GMS/Granite	3	(6)	0.00±0.04	-0.02±0.05	73.97	1.02	0.71	40.4	0.025	29.8
Mpageni	2.74 (a)	Bar-12	GMS/Granite	3	(6)	+0.04±0.06	+0.01±0.03	70.80	0.53	0.58	46.5	0.055	9.4
		99/111	GMS/Granite	3	(8)	-0.14±0.05	-0.06±0.03	74.30	0.73	0.55	54.3	0.050	8.7
Piggs Peak	3.12 (g)	Bar-14	GMS/Granite	3	(7)	+0.04±0.05	+0.02±0.01	70.62	1.76	0.79	22.7	0.056	36.7
		Bar-15	GMS/Granite	3	(5)	+0.02±0.02	0.00±0.01	70.60	1.72	0.83	41.8	0.026	52.8
Salisbury Kop	3.11 (a)	99/115	GMS/Granite	3	(7)	+0.04±0.05	+0.02±0.03	72.77	0.65	0.80	20.9	0.043	28.5
		Bar-13	GMS/Granite	3	(6)	+0.05±0.07	+0.02±0.03	74.34	1.62	0.75	30.7	0.059	13.1
Stentor	3.11 (a)	99/117	GMS/Granite	3	(6)	-0.08±0.04	-0.03±0.03	77.34	0.96	0.27	5.88	0.039	0.84
		Bar-7	GMS/Granite	4	(6)+[6]	-0.08±0.05	-0.03±0.02	74.15	0.84	0.75	39.2	0.036	20.3
Mpuluzi	3.11 (a)	99/126	GMS/Granite	3	(6)	-0.02±0.06	+0.02±0.04	72.29	0.81	0.53	8.12	0.060	8.7
		99/127	GMS/Granite	3	(6)	-0.05±0.06	-0.03±0.01	70.00	0.89	0.41	41.2	0.048	6.8
		Bar-1	GMS/Granite	4	(6)+[6]	-0.05±0.06	-0.03±0.03	69.08	1.11	0.41	42.2	0.051	7.0
Sinceni	3.07 (h)	SINC1	GMS/Granite	3	(6)	-0.04±0.04	0.00±0.02	74.05	1.70	0.17	17.0	0.078	1.7
		SINC2	GMS/Granite	3	(10)	-0.04±0.06	-0.02±0.02	74.88	1.65	0.17	14.8	0.082	1.6
Nhlangano	2.98 (i)	SW5-1	GMS/Granite	3	(6)	-0.09±0.07	-0.05±0.03	73.62	2.49	0.33	10.6	0.058	0.23
Ncotshane gneiss	2.81(j)	MG 18	GMS/Granite	3	(7)	-0.10±0.06	-0.06±0.02	73.13	2.10	0.44	5.37	0.090	0.40
		MG 35	GMS/Granite	3	(6)	-0.04±0.02	-0.01±0.03	78.79	3.19	0.09	11.3	0.074	0.34
Mbabane	2.69 (k)	Bar-16	GMS/Granite	3	(6)	-0.10±0.05	-0.03±0.03	73.70	1.71	0.40	22.9	0.076	3.9
		BHVO-1	Geostan./Basalt	2	[6]	-0.30±0.03	-0.15±0.02	49.94					
		BHVO-2	Geostan./Basalt	6	(25)+[12]	-0.29±0.03	-0.14±0. 02	49.90					
		GA	Geostan./I-type granite	7	(70)+[6]	-0.24±0.02	-0.12±0.01	69.9					
			Diatomite standard	7	(79)+[9]	+1.26±0.02	+0.65±0.01						

*Corresponding author

Supplementary Table 2 legend

References : (a) Kamo & Davis (1994) ; (b) Kröner et al., (1996) ; (c) Kröner et al., (2016) ; (d) Kröner et al., (1991); (e) Kisters et al., (2010); (f) Schoene et al. (2008); (g) (Murphy (2015); (h) Maphalala and Kröner (1993); (i) Hofmann et al. (2015); (j) Dlamini et al. (2017); (k) Layer et al. (1989).

n : Number of full chemical replicates starting from a new powder; (∗) Number of solution analysed with the Nu instrument ; [∗∗] Number of solutions analyzed with the Neptune instrument . Standard reference $\delta^{30}Si$, $\delta^{29}Si$ $\pm 2\sigma_X$ values : BHVO-1 (-0.30±0.05‰, -0.16±0.02‰, Savage et al., 2014); BHVO-2 (-0.30±0.09‰, -0.15±0.04‰, Savage et al., 2014); GA (-0.25±0.03‰, -0.12±0.01‰, Poitrasson & Zambardi, 2015) ; Diatomite (+1.26±0.02‰, +0.64±0.02‰, Reynolds et al., 2007).

Supplementary Table 2 references

Dlamini N., Hofmann, A., Belyanin, G., Xie, H., Kröner, A., Wilson, A., Slabunov, A. (2017). Supracrustal gneisses in southern Swaziland: a basalt-sandstone assemblage of the upper Mozaan Group deformed in the Neoarchaean. South African Journal of Geology 120, 477-498. doi:10.25131/gssajg.120.4.477

Hofmann, A., Kröner, A., Xie, H., Hegner, E., Belyanin, G., Kramers, J., Bolhar, R., Slabunov, A., Reinhardt, J. and Horváth, P., (2015). The Nhlangano gneiss dome in south-west Swaziland–a record of crustal destabilization of the eastern Kaapvaal craton in the Neoarchaean. Precambrian Research, 258, pp.109-132.

Kamo, S.L, Davis, D.W. (1994). Reassessment of Archean crustal development in the Barberton Mountain Land, South Africa, based on U-Pb dating. Tectonics, 13, 167-192.

Kröner, A., Byerly, G.R., Lowe, D.R. (1991). Chronology of early Archaean granite-greenstone evolution in the Barberton Mountain Land, South Africa, based on precise dating by single zircon evaporation. Earth and Planetary Science Letters, 103, 41-54.

Kröner, A., Hegner, E., Wendt, J.I., Byerly, G.R. (1996). The oldest part of the Barberton granitoid-greenstone terrain, South Africa: evidence for crust formation between 3.5 and 3.7 Ga. Precambrian Research, 78, 105-124.

*Corresponding author

Kröner, A., Anhaeusser, C.R., Hoffmann, J.E., Wong, J., Geng, H., Hegner, E., Xie, H., Yang, J. and Liu, D., (2016). Chronology of the oldest supracrustal sequences in the Palaeoarchaean Barberton Greenstone Belt, South Africa and Swaziland. Precambrian Research, 279, pp.123-143.

Layer, P. W., Kröner, A., McWilliams, M., & York, D. (1989). Elements of the Archean thermal history and apparent polar wander of the eastern Kaapvaal Craton, Swaziland, from single grain dating and paleomagnetism. Earth and Planetary Science Letters, 93(1), 23-34.

Maphalala, R.M., Kröner, A., (1993). Pb-Pb single zircon ages for the younger Archean granitoids of Swaziland, southern Africa. In: Maphalala, R., Mabuza, M. (compilers): Extended Abstract of the International Colloquium on African Geology (16th). Geological Survey and Mines Department (Swaziland), 201–206.

Poitrasson F. & Zambardi T. An Earth–Moon silicon isotope model to track silicic magma origins. Geochim. Cosmochim. Acta 167, 301–312 (2015).

Reynolds, B.C., Aggarwal,J., André , L., Baxter,D., Beucher,C., Brzezinski, M.A., Engstrom, E., Georg,R.B., Land,M., Leng,M.J., Opfergelt,S., Rodushkin,I., Sloane, J.T.,VanDenBoorn,S.H.J.M.,Vroon,P.Z.,Cardinal,D., (2007). An inter-laboratory comparison of Siisotope reference materials. J.Anal.At.Spectrom.22, 561–568.

Savage, P.S., Armytage, R.M.G., Georg, R.B. & Halliday, A.E. High temperature silicon isotope geochemistry. Lithos 190-191, 500-519 (2014).

Schoene, B., de Wit, M.J., Bowring, S.A. (2008). Mesoarchean assembly and stabilization of the eastern Kaapvaal craton: A structural-thermochronological perspective. Tectonics 27, TC5010, doi:10.1029/2008TC002267

*Corresponding author

Supplementary Table 3 : Average major element (wt%), $\delta^{30}Si$ (‰), K_2O/Na_2O, Lu/Hf, La/Nb, Th/Nb for silicified and unsilicified metabasalts from the Theespruit (Thee.) and Hoogenoeg-Kromberg (Hoog.-Kr.) formations (data from ref. 20, 29) and our proposed source for TTGs (1:3 proportions of Theespruit silicified and unsilicied metabasalts) compared to the average Coucal basalts (C-F2, data from ref. 33,35) and MORBs (data from ref. 49).

	Hoog.-Kr. Unsilicified Metabasalts (n=4 ± 2σx)	Hoog.-Kr. Silicified Metabasalts (n=10 ± 2σx)	Thee. Unsilicified Metabasalts (n=4 ± 2σx)	Thee. Silicified Metabasalts (n=3 ± 2σx)	TTG Proposed source	(C-F2)	N-MORB	E-MORB	D-MORB
SiO_2	46.68±6.36	73.46±7.66	48.64±1.20	73.01±14.87	**54.73**	50.00	50.42	50.58	50.39
TiO_2	1.09±0.16	0.94±0.12	1.53±0.42	1.16±0.68	**1.44**	1.53	1.53	1.53	1.51
Al_2O_3	13.85±1.26	11.52±1.30	10.23±3.68	10.52±2.86	**10.30**	13.77	15.13	14.94	14.93
Fe_2O_3	16.38±2.82	2.87±2.38	18.01±1.20	8.03±8.88	**15.51**	13.89	10.90	10.71	11.28
MnO	0.23±0.04	0.05±0.04	0.31±0.08	0.39±0.52	**0.33**	0.24	0.17	0.17	0.18
MgO	7.93±3.12	1.33±0.68	6.72±2.96	2.36±2.46	**5.63**	3.80	7.76	7.37	7.82
CaO	6.41±3.52	1.99±1.60	11.01±3.90	0.84±0.38	**8.47**	7.67	11.35	11.18	11.49
Na_2O	0.71±0.52	0.20±0.16	2.46±0.98	1.42±1.06	**2.20**	2.77	2.83	2.72	2.71
K_2O	1.65±1.30	2.91±0.82	0.14±0.08	0.60±0.64	**0.25**	0.52	0.14	0.39	0.10
P_2O_5	0.07±0.02	0.04±0.02	0.14±0.06	0.09±0.12	**0.08**	0.30	0.16	0.24	0.15
LOI	5.10±2.34	4.66±1.82	2.50±2.54	1.92±1.08	**2.36**	6.49	-	-	-
$\delta^{30}Si$	-0.43±0.16	+0.45±0.18	-0.18±0.16	+0.36±0.14	**0.00**	-	-	-	-
K_2O/Na_2O	2.32	14.6	0.06	0.42	**0.11**	0.19	0.050	0.145	0.035
Lu/Hf	0.229±0.016	0.121±0.038	0.118±0.008	0.109±0.010	**0.117**	0.121	0.195	0.150	0.217
La/Nb	0.916	1.029	0.980	1.358	**1.075**	1.503	1.158	0.704	1.300
Th/Nb	0.086	0.104	0.064	0.054	**0.062**	0.180	0.070	0.065	0.080

*Corresponding author

Supplementary Table 4. Comparison Nu and Neptune MC-ICP-MS $\delta^{30}Si$ determinations on Bar 1 to 10 specimens.

(3 measures a,b,c on four different powder aliquots 1 to 4)

Nu		Neptune*		
Aliquot	$\delta^{30}Si$ (‰)	Aliquot	$\delta^{30}Si$ (‰)	ΔNu-Neptune (‰)
Bar1-1a	-0.10	Bar1-3a	-0.16	
Bar1-1b	-0.10	Bar1-3b	-0.19	
Bar1-1c	-0.07	Bar1-3c	-0.10	
Bar1-2a	-0.06	Bar1-4a	0.02	
Bar1-2b	0.01	Bar1-4b	0.10	
Bar1-2c	-0.08	Bar1-4c	0.13	
mean	-0.07		-0.03	-0.04
2sd	*0.08*		*0.28*	
Bar2-1a	-0.16	Bar2-3a	-0.16	
Bar2-1b	-0.07	Bar2-3b	-0.06	
Bar2-1c	0.04	Bar2-3c	-0.15	
Bar2-2a	-0.08	Bar2-4a	0.13	
Bar2-2b	-0.09	Bar2-4b	0.12	
Bar2-2c	-0.11	Bar2-4c	0.04	
mean	-0.08		-0.01	-0.07
2sd	*0.15*		*0.26*	
Bar3-1a	0.05	Bar3-3a	-0.07	
Bar3-1b	-0.04	Bar3-3b	-0.01	
Bar3-1c	0.09	Bar3-3c	0.04	
Bar3-1a	-0.12	Bar3-4a	-0.04	
Bar3-1b	-0.17	Bar3-4b	0.10	
Bar3-1c	-0.05	Bar3-4c	0.04	
mean	-0.04		0.01	-0.05
2sd	*0.20*		*0.13*	
Bar5-1a	0.09	Bar5-3a	-0.14	
Bar5-1b	-0.10	Bar5-3b	0.01	
Bar5-1c	-0.06	Bar5-3c	0.06	
Bar5-2a	-0.05	Bar5-4a	-0.11	
Bar5-2b	0.00	Bar5-4b	-0.04	
Bar5-2c	0.09	Bar5-4c	0.10	
mean	0.00		-0.02	0.02
2sd	*0.16*		*0.19*	
Bar6-1a	-0.05	Bar6-3a	-0.01	
Bar6-1b	-0.03	Bar6-3b	0.14	
Bar6-1c	-0.01	Bar6-3c	-0.13	
Bar6-2a	0.08	Bar6-4a	-0.10	
Bar6-2b	-0.17	Bar6-4b	-0.17	

*Corresponding author

Bar6-2c	-0.16	Bar6-4c	0.17	
mean	-0.06		-0.02	-0.04
2sd	*0.19*		*0.28*	
Bar7-1a	-0.03	Bar7-3a	0.01	
Bar7-1b	-0.20	Bar7-3b	-0.08	
Bar7-1c	-0.14	Bar7-3c	-0.04	
Bar7-1a	-0.07	Bar7-4a	-0.15	
Bar7-1b	0.12	Bar7-4b	-0.14	
Bar7-1c	-0.08	Bar7-4c	-0.13	
mean	-0.07		-0.09	0.02
2sd	*0.22*		*0.13*	
Bar8-1a	-0.15	Bar8-3a	0.01	
Bar8-1b	-0.03	Bar8-3b	-0.10	
Bar8-1c	-0.02	Bar8-3c	-0.05	
Bar8-2a	-0.08	Bar8-4a	-0.05	
Bar8-2b	-0.05	Bar8-4b	0.00	
Bar8-2c	-0.11	Bar8-4c	-0.11	
mean	-0.07		-0.05	-0.02
2sd	*0.17*		*0.10*	
Bar9-1a	-0.11	Bar9-3a	-0.02	
Bar9-1b	-0.10	Bar9-3b	-0.08	
Bar9-1c	0.00	Bar9-3c	0.05	
Bar9-2a	0.05	Bar9-4a	0.04	
Bar9-2b	-0.19	Bar9-4b	0.01	
Bar9-2c	-0.04	Bar9-4c	-0.08	
mean	-0.06		-0.01	-0.05
2sd	*0.17*		*0.12*	
Bar10-1a	-0.01	Bar10-3a	-0.05	
Bar10-1b	0.08	Bar10-3b	-0.03	
Bar10-1c	0.14	Bar10-3c	-0.10	
Bar10-2a	0.08	Bar10-4a	-0.04	
Bar10-2b	-0.05	Bar10-4b	0.01	
Bar10-2c	0.10	Bar10-4c	0.04	
mean	0.05		-0.03	0.08
2sd	*0.14*		*0.10*	

* The measurements on the Neptune (IFREMER, Brest, France) were realized on solutions prepared in Belgium in parallel to the Nu measured solutions. They were managed by G. Ponzevera and G.Bayon from Ifremer.

*Corresponding author

Supplementary Table 5 : Major (in wt%) and trace (in ppm) elements for unpublished specimens

Pluton	Steynsdorp	Stolzburg	Theespruit	Badplaas	Nelshoogte	Kaap Valley
Sample	Bar-6	Bar-2	Bar-3	Bar-5	Bar-9	Bar-8
SiO_2	71.78	73.64	71.09	70.59	71.8	64.12
TiO_2	0.31	0.15	0.23	0.24	0.27	0.51
Al_2O_3	14.79	14.5	15.21	15.84	14.99	15.52
FeOT	2.55	1.25	1.96	2.2	2.16	4.4
MnO	0.04	0.02	0.03	0.03	0.03	0.06
MgO	0.56	0.3	0.87	0.72	0.69	2.7
CaO	2.36	1.66	2.2	3.05	2.85	4.5
Na_2O	4.7	5.13	5.5	5.28	4.98	4.65
K_2O	2.16	2.62	2.01	0.81	1.28	1.16
P_2O_5	0.07	0.03	0.06	0.08	0.08	0.16
LOI	0.51	0.26	0.58	0.98	0.53	2.25
Total	99.83	99.55	99.75	99.8	99.66	100.04
V	16.40	6.6	16.3	13.9	20.4	76.6
Co	109	98.3	114	113	101	70.8
Ga	21.0	16.1	19.4	15.9	17.1	17.7
Rb	53.2	51.7	75.4	28.4	37.2	32.8
Y	13.80	2.2	6.21	2.59	2.56	7.27
Sr	301	502	495	521	498	499
Y	13.80	2.2	6.21	2.59	2.56	7.27
Zr	106	44.8	111	91	106	59.9
Nb	8.98	2.67	6.01	2.48	2.17	3.68
Cs	3.30	1.45	2.46	0.71	1.52	2.23
Ba	391	1165	387	122	164	204
La	23.60	9.29	18.9	14.2	24	22.4
Ce	47.20	18.0	33.8	27.4	45.6	45.4
Pr	4.86	1.94	3.33	2.66	4.3	4.58
Nd	17.80	6.81	11.3	9.14	14.3	16.3
Sm	3.22	1.11	1.99	1.4	1.97	2.7
Eu	0.78	0.35	0.51	0.48	0.62	0.88
Gd	2.72	0.76	1.56	0.92	1.1	2.16
Dy	2.40	0.42	1.11	0.56	0.57	1.46
Ho	0.50	0.08	0.22	0.09	0.1	0.29
Er	1.33	0.19	0.58	0.26	0.27	0.7
Yb	1.29	0.17	0.66	0.22	0.24	0.67
Lu	0.20	0.03	0.1	0.03	0.05	0.09
Hf	2.87	1.45	3.42	2.34	2.64	1.67
Pb	8.99	1.55	8.22	2.12	3.11	2.42
Th	5.87	1.74	6.33	2.03	2.59	2.65
U	1.10	0.49	2.08	0.3	1.68	0.6

*Corresponding author

Pluton	Dalmein	Nelspruit	Mpageni	Piggs Peak	Piggs Peak	Salisbury Kop
Sample	Bar-10	BAR11	BAR12	BAR 14	BAR 15	Bar-13
SiO_2	70.4	73.97	70.8	70.62	70.6	74.34
TiO_2	0.31	0.226	0.299	0.453	0.454	0.103
Al_2O_3	14.85	13.68	15.09	13.67	13.7	13.43
FeOT	2.33	1.608	2.759	3.501	3.456	1.309
MnO	0.05	0.065	0.088	0.066	0.066	<0.05
MgO	0.75	0.337	0.701	0.458	0.449	0.098
CaO	1.9	1.092	2.18	1.587	1.593	0.735
Na_2O	4.99	4.131	4.793	3.139	3.164	3.296
K_2O	2.72	4.224	2.553	5.51	5.457	5.327
P_2O_5	0.15	0.078	0.149	0.139	0.141	<0.05
LOI	1.15	0.44	0.51	0.35	0.32	0.59
Total	99.62	99.85	99.92	99.49	99.4	99.23
V	25	24	12	34	36	20
Co	108	3.3	0.9	4.1	5.5	3.4
Ga	18.1	17.6	14.2	20.6	16.9	15.5
Rb	91.1	115	203	131	157	133
Y	12.3	10.3	26.8	17.7	18.2	20.8
Sr	479	307	251	649	960	273
Y	12.3	10.3	26.8	17.7	18.2	20.8
Zr	128	216	245	117	300	129
Nb	10.8	11.4	26.9	8.9	10.2	10.1
Cs	1.79	1.9	2	8.9	4.6	4
Ba	574	664	765	512	1602	523
La	51.3	53.2	166	44.4	73.6	71.8
Ce	103	108	307	82.3	155	86.9
Pr	10.2	11.02	28.55	8.65	17.04	12.44
Nd	33.8	38.2	85.9	31	63.9	44.5
Sm	5.25	6.5	11.84	5.47	10.37	6.27
Eu	1.37	1.27	1.78	1.27	2.38	1.4
Gd	3.72	4.65	7.55	4.42	7.46	5.17
Dy	2.36	2.43	4.99	3.45	4	3.37
Ho	0.48	0.43	0.9	0.66	0.61	0.61
Er	1.15	1.05	2.48	1.7	1.46	1.66
Yb	1.11	0.89	2.41	1.32	1.19	1.58
Lu	0.17	0.14	0.34	0.19	0.18	0.24
Hf	3.37	5.7	6.2	3.4	6.9	4.1
Pb	3.05					
Th	8.88	7.9	40	10.6	8.5	9.3
U	2.42	0.9	7.5	2.7	1.9	2.8

*Corresponding author

Pluton	Stentor	Mpuluzi	Sinceni	Sinceni	Mbabane
Sample	Bar7	Bar-1	SINC1	SINC2	Bar-16
SiO_2	74.15	69.08	74.05	74.88	73.7
TiO_2	0.15	0.51	0.16	0.10	0.16
Al_2O_3	13.94	14.52	13.76	13.63	13.77
FeOT	1.59	3.31	1.74	1.38	1.76
MnO	0.04	0.07	0	0	<0.05
MgO	0.18	0.6	0.12	0.09	0.13
CaO	0.88	1.49	0.84	0.75	0.84
Na_2O	4.49	4.03	3.25	3.26	3.24
K_2O	3.77	4.46	5.53	5.37	5.54
P_2O_5	0.03	0.16	0.05	0.00	0.05
LOI	0.47	0.93	0.44	0.48	0.71
Total	99.7	99.18	99.93	99.93	99.91
V	5.85	25.1	12	9	21.0
Co	112	87.5	1.1	0.9	4.90
Ga	17.5	23	19.4	19.6	17.40
Rb	127	230	422	374	277
Y	12	33.8	31.5	34.1	59.7
Sr	244	236	53.7	55.2	234
Y	12	33.8	31.5	34.1	59.70
Zr	150	318	161	162	415
Nb	10.4	46.6	31	32.2	39.0
Cs	3.97	5.35	29.3	14.2	5.70
Ba	913	1190	227	235	875
La	62	168	68.5	68.7	190
Ce	121	337	143	142	344
Pr	12.4	32.5	14.57	14.72	32.85
Nd	42.4	104	49.7	50.1	106
Sm	6.82	15.6	9.23	9.03	15.74
Eu	1.35	1.72	0.45	0.45	1.87
Gd	4.44	10.6	7.35	7.65	12.91
Dy	2.56	7.61	6.33	6.81	10.56
Ho	0.46	1.35	1.2	1.28	2.17
Er	1.1	3.24	3.11	3.35	6.42
Yb	1.07	2.69	2.72	3.14	5.62
Lu	0.17	0.38	0.43	0.45	0.82
Hf	4.69	7.44	5.5	5.5	10.80
Pb	8.06	8.9			
Th	18.1	15.5	36.9	35.5	54.2
U	2.58	3.06	9.8	10.2	7.80

*Corresponding author